Technical Note	LIGO-T1700196–v3	2017/09/22

Laser Mode Spectroscopy for Mirror Metrology

LIGO SURF Final Report

Naomi Wharton
Mentors: Koji Arai and Rana Adhikari

1   Abstract

The LIGO gravitational wave detectors are specialized Michelson interferometers each with two arms that are four kilometers in length. Each arm of the interferometers forms an optical cavity capped by semi-transparent mirrors by which laser light is transmitted and reflected. Imperfections on the surfaces of these mirrors cause optical power losses in the cavities that must be minimized for optimal performance. In a cavity with perfectly spherical mirrors, the modes of a Gaussian beam will resonate at equally spaced frequencies. In reality, surface perturbations cause the resonance peaks of several higher-order (Hermite-Gaussian) modes to shift in the cavity transmission spectrum. The aim of this project is to use cavity scan techniques to measure deviations in the spacing of these higher-order modes. By comparing these experimental deviations with theoretical mode spacings, we can learn about the physical properties of the cavity mirrors. Our ultimate goal is to use Bayesian inference techniques to recreate the surface perturbation map of a mirror from its cavity transmission spectrum.

2 Introduction

2.1 Einstein's Gravitational Waves

Our knowledge of the universe derives almost exclusively from observations of electromagnetic waves. For centuries, early astronomers used optical telescopes to continually reshape humanity's understanding of the size and structure of the world beyond Earth. The twentieth century brought significant technological advances that allowed us to peer at the universe in a different light, outside of the visible spectrum; observations in the radio, infrared, ultraviolet, x-ray, and gamma ray portions of the electromagnetic spectrum revealed knowledge previously hidden by our own eyes.

Gravitational wave astronomy offers a fundamentally different tool by which to learn about the universe. Instead of *looking* for electromagnetic waves traveling through space, we are *listening* for light-speed vibrations in spacetime itself. Originally predicted as a consequence of Einstein's general theory of relativity in 1915, gravitational waves were first observed by the Laser Interferometer Gravitational-Wave Observatory (LIGO) on September 14, 2015.

2.2 Gravitational Wave Detection

As a gravitational wave propagates through spacetime at the speed of light, it alters the relative length between objects with mass. These differential changes in length are normally impossibly small to detect. However, when the source of a gravitational wave is as massive and compact as the merger of a binary black hole system, the differential length change is large enough to detect with an extremely sensitive interferometer.

The Advanced LIGO gravitational wave detectors in Hanford, WA, and Livingston, LA, are specialized Michelson interferometers each with two arms that are four kilometers in length. Each arm of the interferometers forms a Fabry-Pérot cavity capped by a semi-transparent Input Test Mass (ITM) and an End Test Mass (ETM). Gravitational waves that pass through the detectors slightly alter the relative distance between the corresponding test masses; interferometers are able to convert these differential changes in length into an optical signal [1].

2.3 Optical Loss

As laser light passes into the Fabry-Pérot cavities, it is continually transmitted and reflected by the semi-transparent mirrors. The LIGO interferometers use these Fabry-Pérot cavities in order to increase the interaction time between a passing gravitational wave and the detector [3]. In order to maintain the sensitivity of the interferometer to gravitational waves, it is essential that the cavities have a low optical power loss. Several of the factors that contribute to the power loss in the cavity are:

- figure error of the test masses

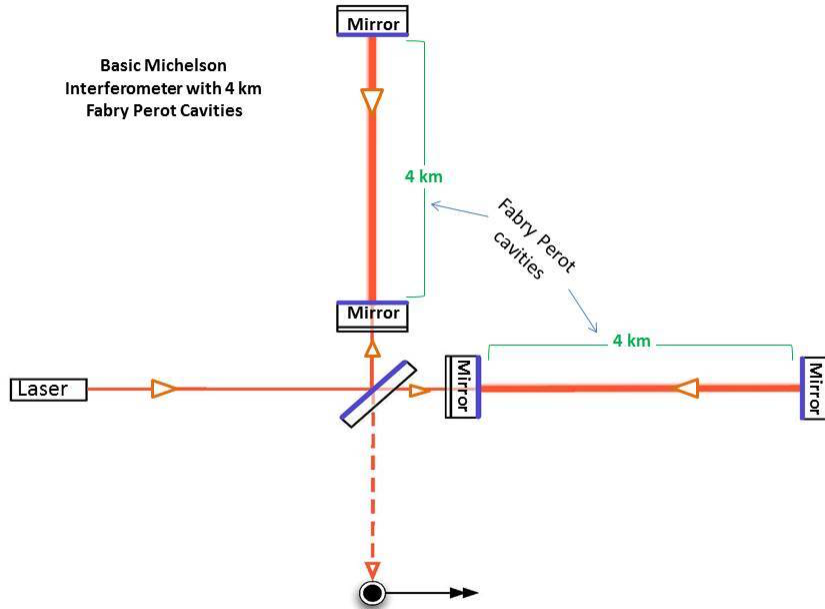- defects - surface aberrations, scratches, point defects, contamination

Figure 1: Basic 4-km Michelson interferometer. Source: [2]

- absorption by test mass coatings

- microroughness of the test masses

- transmission by the ETM

In order for the LIGO interferometers to function effectively, the round trip cavity loss must be less than 75 parts per million [3]. Thus, it is of great interest to LIGO science to understand and be able to categorize the sources of optical loss in the Fabry-Pérot cavities of gravitational wave detectors.

The main goal of this project is to evaluate optical loss in a gravitational wave interferometer due to mirror figure error. Currently, a Fizeau interferometer can be used to produce a phase map of mirror surfaces as they are being polished and coated [3]. However, this can only be performed outside of the actual detectors. We want to instead be able to perform an *in-situ* interferometric measurement of the mirror figure error with the cavity beam actually used for gravitational wave detection.

3 Objectives

3.1 Project Outline

In this project, we will use cavity scan techniques to measure deviations of the transverse Hermite-Gaussian modes (see Section 3.3) of an optical cavity from their ideal equal spacing

(14). By comparing these experimental deviations with theoretical mode spacings, we hope to learn information about the shape of the cavity mirror, allowing us to characterize the sources of optical loss in the cavity. Our ultimate goal is thus to be able to create a "mirror map" of the imperfections of a cavity mirror using measurements of the higher-order modes that resonate within the cavity.

In the following subsections, we will introduce the relevant concepts and terminology relating to optical cavities and their properties.

3.2   Fabry-Pérot Cavity Modes [4]

A Fabry-Pérot cavity, or resonator, is a simple setup of two flat, parallel mirrors separated by a distance L. The electromagnetic modes $U(\mathbf{r})$ of a Fabry-Pérot resonator are the solutions of the Helmholtz equation,

$$\nabla^2 U + k^2 U = 0, \tag{1}$$

given the boundary conditions defined by the two reflective surfaces. If the two mirrors are positioned perpendicularly along the z-axis, with the first mirror at $z = 0$ and the second mirror at $z = d$, we can write these longitudinal modes as standing waves with complex amplitude

$$U(\mathbf{r}) = A_q \sin k_q z, \tag{2}$$

where q is an integer, A_q is a constant coefficient corresponding the the qth mode, and k_q is the wavenumber given by

$$k_q = \frac{q\pi}{L}. \tag{3}$$

This ensures that the complex amplitude vanishes at both $z = 0$ and at $z = L$, as dictated by our boundary conditions. From Equation (3), we can find that the frequency of the qth mode is given by

$$\nu_q = \frac{ck}{2\pi} = \frac{c}{2\pi}\left(\frac{q\pi}{L}\right) = \frac{qc}{2L}, \tag{4}$$

where c is the speed of light in the medium. Each resonant frequency ν_q is thus separated from adjacent resonant frequencies $\nu_{q\pm1}$ by

$$\nu_{\text{FSR}} = \frac{c}{2L}. \tag{5}$$

The quantity ν_{FSR} is known as the **free spectral range** of the cavity.

The equal spacing of these longitudinal modes arises if there is no linear dispersion in either the cavity mirrors or the cavity medium. This is conveyed in our use of Equation (4), which implies that the speed of the waves is independent of frequency, ν, and wavenumber, k [5]. We make a note here that the free spectral range ν_{FSR} is determined by the absolute length of the optical cavity, as shown by Equation (5). Thus, just as we can predict ν_{FSR} given the length L of an optical cavity, we can use a measurement of ν_{FSR} to learn about the length of a cavity.

3.3 Hermite-Gaussian Modes [4]

We consider now a spherical-mirror resonator, which consists of two spherical mirrors of radii R_1 and R_2, instead of the planar mirrors of the Fabry-Pérot cavity. Now, the modes of the resonator are paraxial waves - beams whose wavefronts make small angles with the axis of propagation. In particular, a Gaussian beam is a paraxial wave with its power concentrated in a cylinder around the axis of propagation and with its intensity distributed in a Gaussian function centered in the transverse plane. A Gaussian beam is a mode of a spherical-mirror resonator if the radii of curvature of the wavefronts of the beam are the same as the radii of curvature of the spherical mirrors.

A Gaussian beam is the lowest-order solution of a family of solutions to the paraxial Helmholtz equation. These solutions are know as Hermite-Gaussian modes. These beams are similar to Gaussian beams in that they have the same wavefronts, but have different intensity distributions. Instead of the circularly symmetric Gaussian intensity distribution innate to a Gaussian beam, a Hermite-Gaussian beam is characterized by two indices (l, m), which indicate spatial dependencies in the x and y directions, respectively. The complex amplitude of a Hermite-Gaussian beam is often written as

$$U_{l,m}(\mathbf{r}) = A_{l,m}\left[\frac{W_0}{W(z)}\right]G_l\left[\frac{x\sqrt{2}}{W(z)}\right]G_m\left[\frac{y\sqrt{2}}{W(z)}\right]\exp\left[-ikz - ik\frac{x^2+y^2}{2R(z)} + i(l+m+1)\varphi(z)\right], \quad (6)$$

where

$$G_n(u) = H_n(u)\exp\left(\frac{-u^2}{2}\right), \quad n = 0, 1, 2, \ldots \quad (7)$$

is the Hermite-Gaussian function of order n, $H_n(u)$ is the nth-order Hermite polynomial[1], $A_{l,m}$ is a constant, and the following are properties of Hermite-Gaussian beams:

- $R(z)$ is the radius of curvature of the wavefront,

- $W(z)$ is the beam radius along the z-axis,

- W_0 is the beam waist, or minimum spot size of the beam,

- z_R is the Rayleigh range, or the distance along the z-axis at which the wavefronts of the beam are most curved, and is defined as $z_R = \frac{\pi W_0^2}{\lambda}$, and

- $\varphi(z)$ is the Gouy phase shift of the beam, defined as

$$\varphi(z) = \arctan\left(\frac{z}{z_R}\right) \quad (8)$$

We can refer to the Hermite-Gaussian mode with spatial indices (l, m) as TEM_{lm}. The fundamental Gaussian mode is thus referred to as TEM_{00}. The resonance frequencies of the TEM modes are now dependent on these mode indices (l, m), as well as the radii of curvature of the cavity mirrors. Their spacing from the resonance frequencies of the TEM_{00} mode is an

---

[1]See Appendix A.

integer multiple of the *Transverse or Spatial Mode Spacing*, or ν_{TMS} for short. This is given by

$$\nu_{\mathrm{TMS}} = \nu_{\mathrm{FSR}}\left(\frac{l+m}{\pi}\right)\cos^{-1}\sqrt{g_1 g_2}, \tag{9}$$

where $\nu_{\mathrm{FSR}} = \frac{c}{2L}$ as before. The parameters g_1 and g_2 are known as the g-parameters of the cavity, and are defined as

$$g_1 = 1 - \frac{L}{R_1} \ \text{ and } \ g_2 = 1 - \frac{L}{R_2}, \tag{10}$$

where R_1 and R_2 are again the radii of curvature of the cavity mirrors [7]. We can also write Equation (9) as

$$\nu_{\mathrm{TMS}} = \nu_{\mathrm{FSR}}\left(\frac{l+m}{\pi}\right)\Delta\varphi, \tag{11}$$

where $\Delta\varphi$ is the total Guoy phase shift of the cavity, defined as

$$\Delta\varphi = \varphi(z_2) - \varphi(z_1) = \cos^{-1}\pm\sqrt{g_1 g_2}. \tag{12}$$

We can thus write the resonance frequencies of the general spherical-mirror cavity mode as

$$\nu_{lmq} = q\nu_{\mathrm{FSR}} + \left(\frac{l+m+1}{\pi}\right)\nu_{\mathrm{FSR}}\,\Delta\varphi, \tag{13}$$

where q is an integer indicating the longitudinal mode number.

To summarize the spacing of the modes of a spherical-mirror cavity:

1. The different *longitudinal* modes of the cavity are those with the same values of (l, m) but different values of q. As in the Fabry-Pérot cavity, adjacent resonant frequencies are separated by ν_{FSR}; thus, the longitudinal mode spacing is determined by the absolute length of the cavity.

2. Different *transverse* modes are determined by the indices (l, m), which indicate spatial dependencies along the x and y axes, respectively. Adjacent transverse modes with indices (l_1, m_1) and (l_2, m_2), of the longitudinal mode q, are spaced by

$$\nu_{l_1,m_1,q} - \nu_{l_2,m_2,q} = [(l_1 + m_1) - (l_2 + m_2)]\frac{\nu_{\mathrm{FSR}}\,\Delta\varphi}{\pi} \tag{14}$$

   apart. Thus, the spacing of the transverse modes of a cavity depends on the radius of curvature of the cavity mirrors [15]. The intensity distributions of several of the low-order transverse Hermite-Gaussian modes are shown in Figure (2).

In Section (3.2), we noted that by measuring the free spectral range of a cavity, we can determine the cavity's length. Similarly, by measuring the spacing of adjacent transverse modes, we can learn about the radius of curvature of the cavity mirrors. In this project, we explore whether we can use this correlation between mirror radius of curvature and transverse mode spacing as a sensor for mirror figure error.
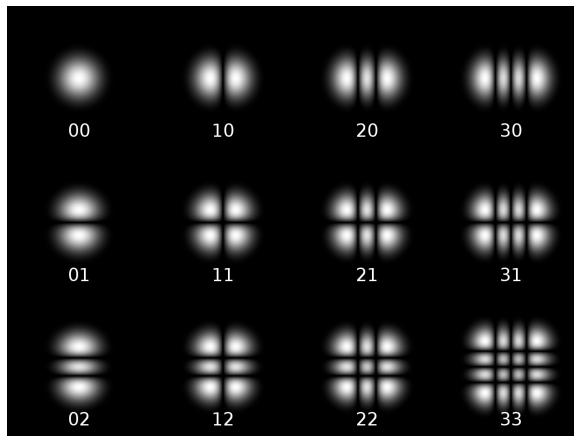
Figure 2: Intensity distributions of several transverse Hermite-Gaussian modes. The indices (l, m) are labeled beneath each mode. We can see that the intensity distribution of the mode with indices (l, m) has l nodes along the horizontal direction and m nodes along the vertical direction.

4   Experimental Methods

Our experimental plan is as follows:

1. Simulation in *Finesse*.

   - Configure *Finesse* (see Section 4.1) to simulate an ideal Fabry-Pérot cavity with the parameters of the LIGO 40m prototype interferometer.

     - Scan the cavity over a range of input frequencies. Plot the transmitted power of the cavity as a function of frequency to observe the resonant transverse modes of the cavity.

   - Introduce a misaligned and mode-mismatched beam into the Fabry-Pérot cavity simulation. Observe the deviations in the transmitted power output from the mode-matched beam. Develop a fitting algorithm to predict the finesse and length of the cavity and the radius of curvature of the cavity mirror based on the cavity transmitted power. Compare these predictions to the simulation settings to evaluate the fitting algorithm.

   - Introduce random figure error to one of the cavity mirrors in the simulation. Observe the effect of this error on the higher order mode spacings of the cavity.

2. Use the knowledge gained in the simulation to create a "mirror map" of a cavity mirror using the results of cavity scan techniques.

   - Generate thousands of potential perturbations in the cavity mirror surfaces and their effect on the optical loss of the cavity. Then, use a Monte Carlo method to try to fit actual cavity scan transmission data to a linear combination of these potential mirror surface perturbations. This will allow us to characterize the sources of optical loss in a cavity as perturbations of the cavity mirrors.

- Use Bayesian inference methods in coordination with the above to predict the probability of loss in a cavity arising from particular perturbations in the cavity mirror surfaces. This involves continually updating the probability of perturbations contributing to the cavity transmission as more information becomes available. Thus, as the fitting algorithm continues, the perturbations that are more likely to be present in the cavity are isolated.

3. Ultimately, apply the above algorithms to actual cavity transmission data from the LIGO 40m prototype interferometer to evaluate mirror figure error.

4.1 Hermite-Gaussian Modes in *Finesse*

To simulate optical cavities, we can use the software package known as *Finesse*, created by GEO 600, to run simulations of user-defined optical cavities [8]. This software allows us to both define our own optical setup and to run scans of these cavities.

To use *Finesse* to simulate an optical cavity, we specify the optical components present and their attributes in an input file with the file extension '.kat'. We begin by simulating a Fabry-Pérot cavity set with the parameters of one arm of the LIGO Caltech 40-meter prototype interferometer. We set the parameters of the optical cavity as follows [9]:

parameter	value
laser wavelength (λ_0)	1064 nm
cavity length (L)	40 m
ITM reflectivity (R)	0.98616
ITM transmissivity (T)	0.01384
ETM reflectivity (R)	0.9999863
ETM transmissivity (T)	$13.7 \cdot 10^{-6}$
ITM radius of curvature (R_1)	∞
ETM radius of curvature (R_2)	57 m

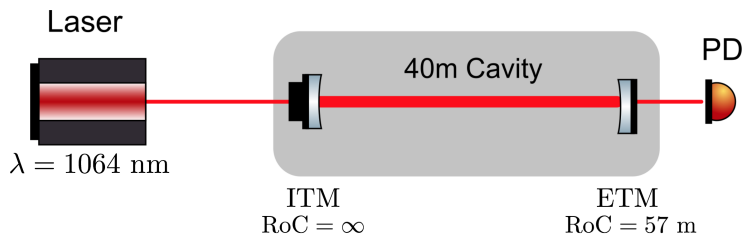Figure (3) shows the setup of our simulated cavity in *Finesse*.

Figure 3: *Finesse* simulation optical setup. A photodetector is placed after the ETM to measure transmitted power.

By default, *Finesse* uses a plane wave approximation of the laser light. We can manually switch to Hermite-Gaussian beams using a command in the input file that specifies the

highest order $(l + m)$ of Hermite-Gaussian modes to be used. We can then individually specify the TEM modes to inject into the cavity, and their relative powers.

We begin with only the fundamental (Gaussian) mode present, TEM_{00}. We set *Finesse* to measure the transmission of the cavity past the second mirror (ETM) using a photodetector, varying the frequency over a range of 20 MHz. Figure (4) shows the resulting plot.
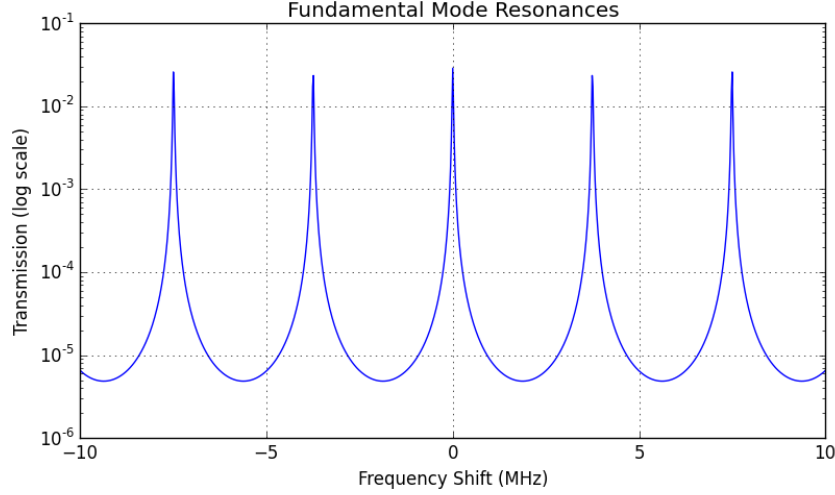

Figure 4: Transmission of 40-meter FP cavity across 20 MHz frequency shifts. Adjacent peaks are separated by ν_{FSR}.

We observe in Figure (4) that adjacent resonant peaks are a distance of

$$\nu_{\text{FSR}} = \frac{c}{2L} \approx 3.75 \text{ MHz} \tag{15}$$

apart, as they are expected to be.

Now, we can insert higher order modes into the cavity and observe their frequency spacing. We can choose to either leave or remove the fundamental TEM_{00} mode; for now, we shall leave the fundamental mode and insert the modes of order 1, each at 50% power relative to the fundamental mode: TEM_{10} and TEM_{01}. Because the simulated optical cavity is not astigmatic, these modes have the exact same resonant frequencies (see Figure 5).

In Figure (5), the first order modes appear as the shorter peaks to the right of the fundamental modes. Each first order peak is once again separated from adjacent first order peaks by a distance of ν_{FSR}. To find the spacing between the fundamental mode and the first order modes, we refer to Equation (9). For both first order modes, we have $l+m = 1$, so transverse mode spacing ν_{TMS} becomes:

$$\nu_{\text{TMS}} = \left(\frac{\nu_{\text{FSR}}}{\pi}\right) \cos^{-1} \sqrt{g_1 g_2} \tag{16}$$

The g-parameters for this cavity are given by:
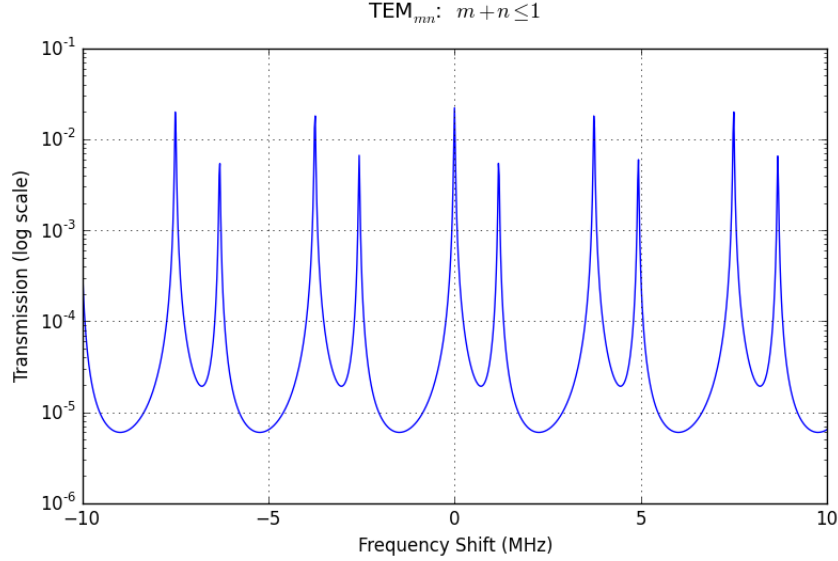
$$g_1 = 1 - \frac{L}{R_1} \approx 1 \tag{17}$$

Figure 5: Transmission of 40-meter FP cavity across 20 MHz frequency shifts. Three modes are present: TEM_{00}, TEM_{10}, and TEM_{01}.

$$g_2 = 1 - \frac{L}{R_2} \approx 0.298 \tag{18}$$

Thus, the transverse mode spacing is given by

$$\nu_{\text{TMS}} = \left(\frac{3.75 \text{ MHz}}{\pi}\right) \cos^{-1} \sqrt{(0.298)}$$

$$\nu_{\text{TMS}} \approx 1.19 \text{ MHz}. \tag{19}$$

We can see in Figure (5) that this is indeed the frequency spacing between the fundamental mode and its corresponding first order mode.

When a laser beam is aligned to a Fabry-Pérot cavity, only the fundamental mode will appear, as in Figure (4). A beam that is misaligned with the cavity will also result in the appearance of several higher-order modes. To represent a misaligned beam in our simulation, we can thus manually insert several higher-order modes using a *Finesse* command. In the simulations for this project, we inserted all modes up to order $l + m \leq 9$. This results in an ideal transmission spectrum as shown in Figure (6).

4.2   Zernike Polynomial Surface Perturbations

The simulated cavity transmission spectra shown in Figures (4), (5), and (6) are calculated with ideal cavity mirrors. In a mirror with figure error, the higher-order mode peaks are shifted from their ideal resonant frequencies.

We can characterize the surface defects of an optical mirror using a phase map. A phase map is essentially a two-dimensional matrix containing the relative height of the surface at a point (x, y) on the mirror. Thus, they show how the path length through which the laser
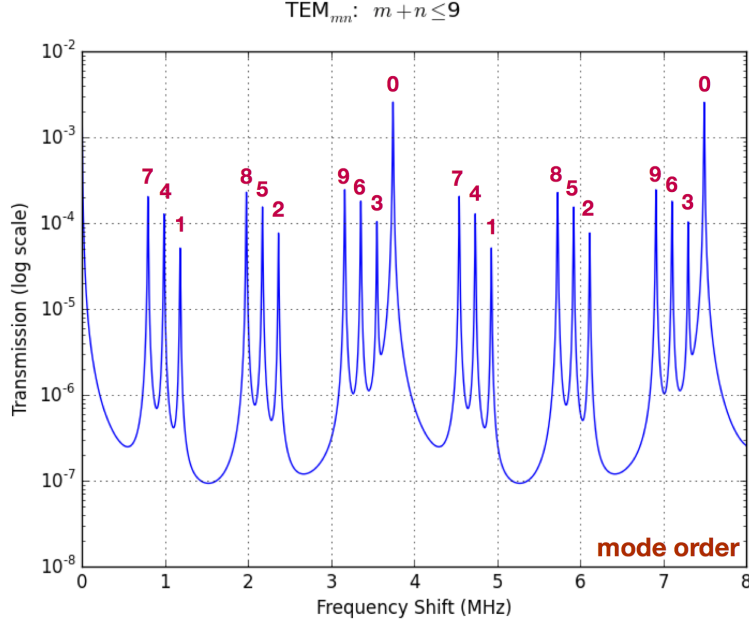
Figure 6: Simulated transmission of 40-meter FP cavity across 8 MHz frequency shifts. All modes up to order $(l+m) \leq 9$ are included. Mode orders are indicated above their respective peaks. As this simulates a perfectly spherical mirror, all modes with the same order (i.e. TEM_{10} and TEM_{01}) have the same resonance frequency and thus appear as one peak.

must propagate varies across the mirror surface. Figure (7) shows an example of a phase map.

To simulate various surface defects on an optical mirror, we can apply perturbations using the Zernike polynomials.[2] The Zernike polynomials are an infinite sequence of polynomials that are orthogonal on the unit disk and are characterized by a radial index, n, and an azimuthal index, m. Each polynomial corresponds to a type of optical aberration. As the Zernike polynomials are linearly independent, individual aberrations can be applied by changing the coefficient of the corresponding polynomial. Figure (8) shows the Zernike polynomials up to order $n = 5$.

We begin by creating a phase map object in *Finesse* and applying it to the ETM. In *Finesse*, the radius of curvature is a property of the mirror object. Thus, adding a flat phase map to the ETM does not affect the perfectly spherical mirror; it is applied as if it were simply added on top of the phase map in Figure (7).

Now, we introduce random perturbations to the phase map by choosing coefficients for the Zernike polynomials from a normal distribution with a standard deviation of 4 nm. For our simulations, we introduced coefficients for the first 120 Zernike polynomials (all polynomials up to and including order $n = 15$). Our phase map now shows variations in surface height on the scale of a few nanometers. These variations in surface height are applied on top of the ETM; thus, while the mirror is still nearly spherical, realistic imperfections now scatter
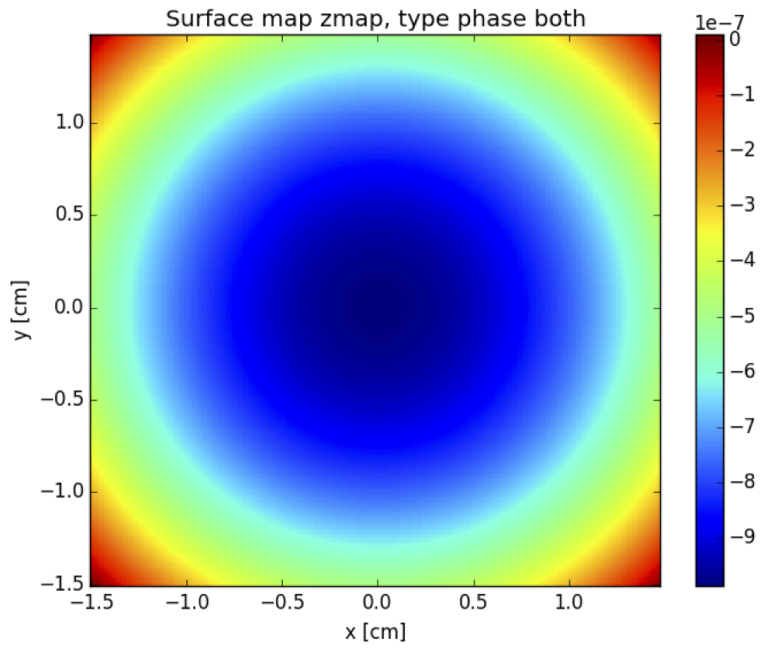
---

[2]See Appendix B.

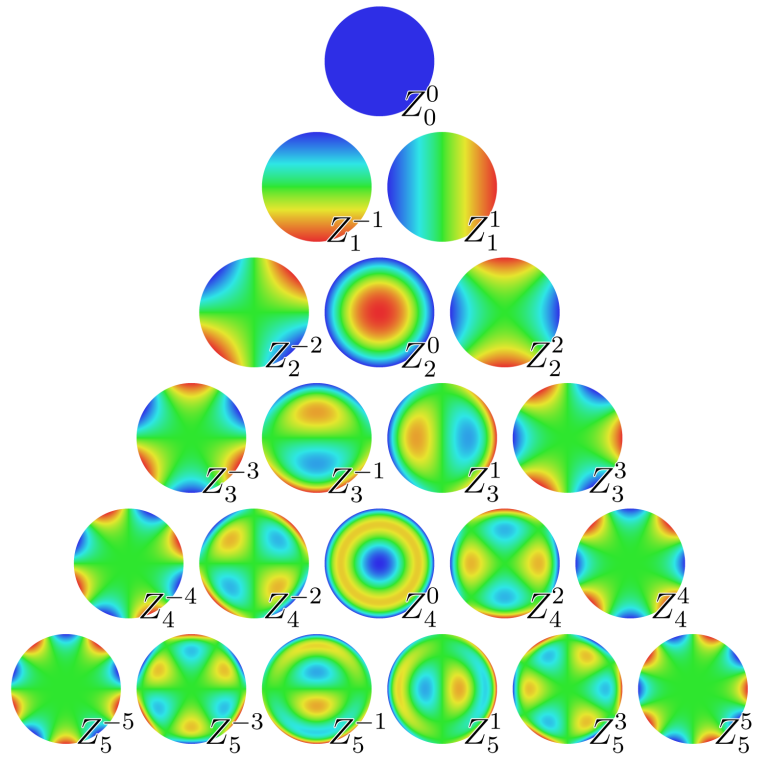Figure 7: Phase map for a perfectly spherical mirror with a radius of curvature of 57 m.

Figure 8: Zernike polynomials up to order $n = 5$.

the surface.

Now, as before, we manually insert all Hermite-Gaussian laser modes into the cavity up to order $(l + m) \leq 9$, giving each higher-order mode a tenth of the power of the fundamental mode. The mirror figure error from the phase map causes the resonance frequencies of the HOMs to shift in the cavity transmission spectrum. Figure (9) shows an example of a mirror map applied to the ETM in our simulation and its corresponding cavity transmission spectrum.
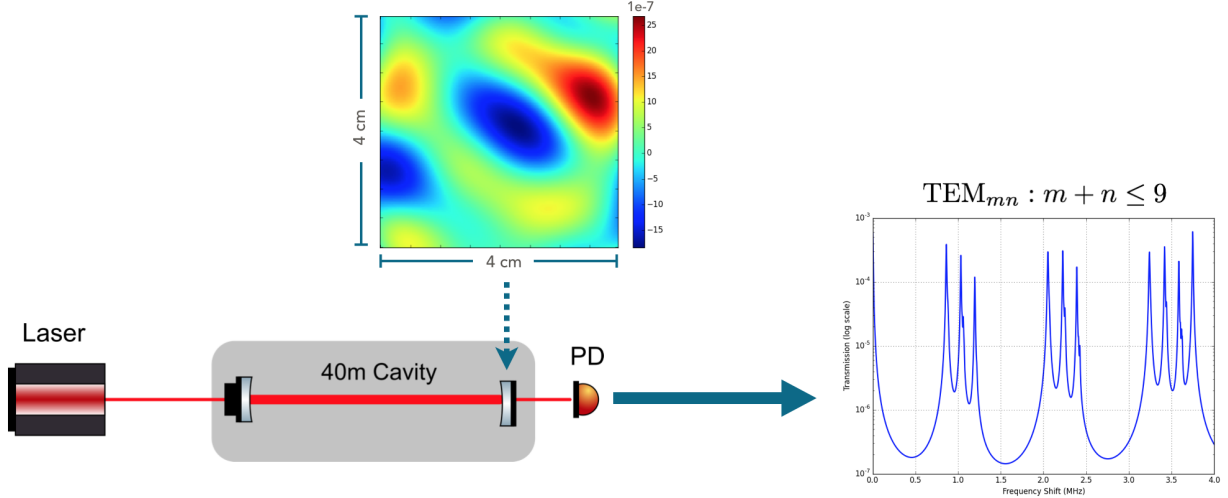

Figure 9: Example of a perturbed mirror map applied to the ETM. Hermite-Gaussian laser modes up to order $n = 9$ are injected into the cavity, and the corresponding cavity transmission spectrum is shown at the right.

If we run this simulation many times, each time generating a new set of normally distributed Zernike coefficients, we can get a sense for how much each HOM shifts with the induced surface perturbations. Figure (10) shows the resulting transmission spectra from 60 random phase maps.

4.3 Shifts in Transverse Mode Spacings

The shifts in the higher-order mode resonance frequencies can tell us some information about the effective cavity parameters resulting from the surface perturbations.

For a given transmission spectrum, we can find both ν_{FSR}, the spacing between adjacent fundamental mode peaks, and ν_{TMS}, the difference in frequency between a higher-order mode peak and the fundamental mode peak. Figure (11) shows how we can read these values off of a transmission spectrum.

As we saw in Section (3.3), ν_{TMS} should vary linearly with Hermite-Gaussian mode order:

$$\nu_{\text{TMS}} = \nu_{\text{FSR}} \left(\frac{l + m}{\pi} \right) \cos^{-1} \sqrt{\left(1 - \frac{L}{R_1} \right) \left(1 - \frac{L}{R_2} \right)} \tag{20}$$
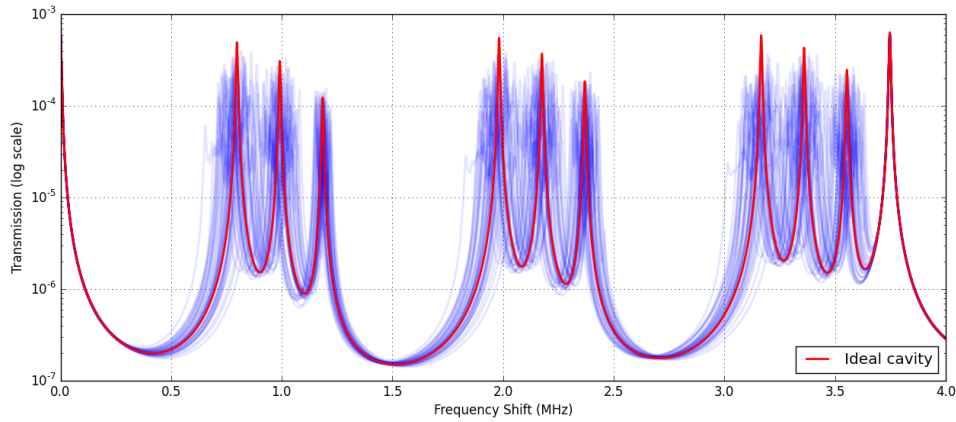
Figure 10: Transmission spectra from 60 phase maps with random Zernike coefficients. The red line shows the transmission spectrum from an ideal cavity.
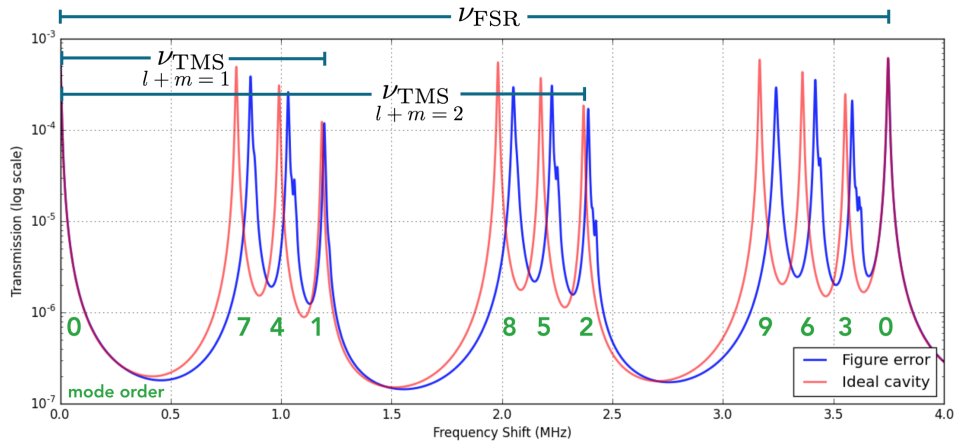

Figure 11: The blue line above shows the transmission spectrum from the phase map in Figure (9), while the red line shows the transmission spectrum from a perfectly spherical mirror. We can see that the blue peaks have shifted horizontally from the ideal red peaks. ν_{FSR} is the frequency spacing between adjacent fundamental peaks, while ν_{TMS} for a given HOM is the frequency spacing between the fundamental mode peak and the higher-order mode peak. ν_{TMS} for modes of orders 1 and 2 are shown in the figure.

We recall that in our setup, $R_1 \approx \infty$. Thus, Equation (20) becomes:

$$\nu_{\text{TMS}} = \nu_{\text{FSR}} \left(\frac{l+m}{\pi} \right) \cos^{-1} \sqrt{\left(1 - \frac{L}{R_2} \right)} \tag{21}$$

From Equation (21), we can see that a change in the radius of curvature of the ETM, R_2, results in a change in ν_{TMS}. However, by introducing figure error to our ETM in the form of Zernike coefficients, we have inadvertently introduced a minute change in the radius of curvature of the mirror. Thus, a slight change in ν_{TMS} is to be expected.

To confirm this, we can perform a linear fit on the shifted ν_{TMS} values and compare them to the ideal ν_{TMS} values. In Figure (12a), a linear fit of the transverse mode spacings for the transmission spectrum in Figure (11) is shown in blue, while the ideal transverse mode spacings are shown in red. The value of ν_{TMS} can be seen in the slope of each line. While the ideal data has a value of

$$\nu_{\text{TMS}} \approx 1.185\,\text{MHz},$$

corresponding to an ETM radius of curvature of 57.0 m, the shifted data has a value of

$$\nu_{\text{TMS}} \approx 1.194\,\text{MHz},$$

corresponding to an effective ETM radius of curvature of 56.44 m.

This correlation between ν_{TMS} and radius of curvature is already well understood. However, the shifted transverse mode peaks do not perfectly align with the expected linear values given the new effective radius of curvature. We can see in Figure (12b) the residuals for this particular linear fit. Here, figure error with a standard deviation of $\sigma = 4$ nm has resulted in a shift of $\approx \pm 5$ kHz from the ν_{TMS} values from our linear fit.
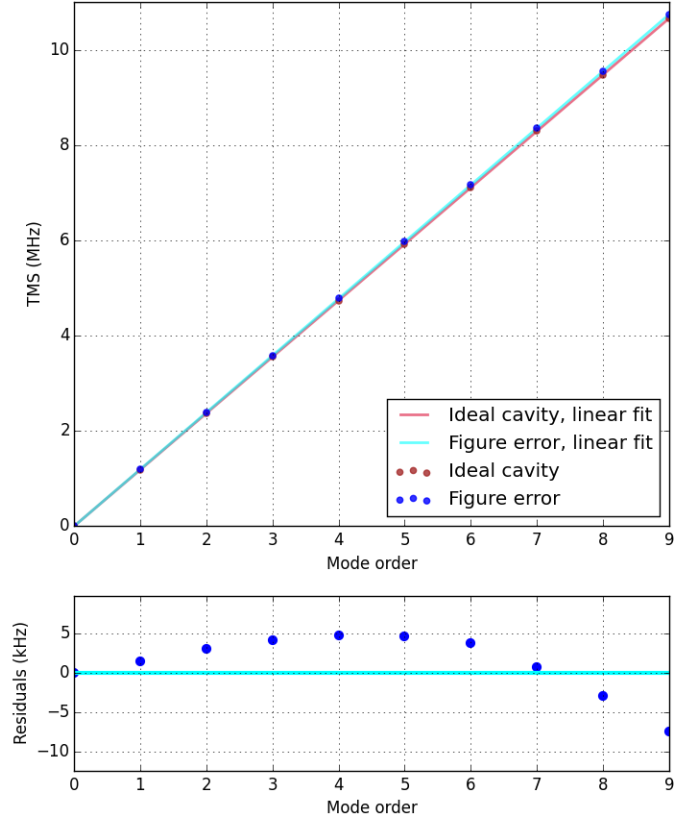

Figure 12: (a, above): Linear fit of ideal transverse mode peak frequencies (red) and transverse mode peaks corresponding to the system with phase map shown in Figure (9) (blue). (b, below): Difference between shifted transverse mode peak frequencies and their linear fit.

4.4 Bayesian Inference Methods

In the above sections, we have shown how figure error of the ETM results in shifts in the transverse mode peak frequencies of a cavity's transmission spectrum. The ultimate goal of this research is to be able to apply this information to cavity scans of LIGO's gravitational wave interferometers in order to learn about mirror figure error of the actual cavity mirrors.

Given a particular mirror surface, we can measure the cavity transmission map relatively easily using an experimental plan such as that described in Section (4.5). The inverse problem - extracting the phase map of a cavity mirror from the transmission data - is significantly harder. In order to extract the phase map, we need to model the dependence of the two quantities (transmission data and surface maps). The ideal next step for this project is thus to run thousands of our simulated cavity scans, each with a different phase map. We would then apply Bayesian inference methods to calculate the most probable phase map (characterized by Zernike polynomial coefficients) given a particular cavity transmission spectrum (characterized by TMS residuals). Below, we discuss how to approach this problem in terms of Bayesian inference methods.

The following paragraphs use the notation of [10]. Let us refer to the cavity transmission data as the random variable Y, the *measurement*, and to the nonobservable phase map as the random variable X, the *unknown*. Before taking a measurement of Y, we have some information about X, which we can use to form the prior probability density $\pi_{\mathrm{pr}}(x)$. We can now express our main problem as: "*Given the data $Y = y_{\mathrm{observed}}$, find the conditional probability distribution $\pi(x \,|\, y_{\mathrm{observed}})$ of the variable X.*"

In other words, given a certain measurement y_{observed} of a cavity's transmission, find the most probable phase map of the cavity mirror. Essential to solving problems of this form is *Bayes' theorem of inverse problems,* which is given in Appendix C.

To solve an inverse problem of this form, we can follow three overarching steps outlined in [10]:

1. Find a prior probability density π_{pr} that reflects all prior information known about the unknown X.

2. Find the *likelihood function,* $\pi(y \,|\, x)$, describing the relationship between the unknown and measured quantities.

3. Develop a method to extract $\pi_{\mathrm{pr}}(x)$, the posterior probability density.

In practice, one method that is commonly used for Bayesian inference is known as *Markov chain Monte Carlo* (MCMC). This relies on the concept of a Markov chain, which is a process with the property that, conditional on its nth step, its future values do not depend on its previous values. MCMC aims to first create a Markov process that has $\pi(x \,|\, y_{\mathrm{observed}})$, the posterior probability distribution of X, as its stationary distribution. We can then run this Markov process long enough such that the resulting output is a close approximation of $\pi(x \,|\, y_{\mathrm{observed}})$. By the law of large numbers, as the sample size n of the approximation increases, the approximation increases in accuracy.

A promising immediate next step for this project is to attempt to implement the above method using the Python **emcee** [13] and/or **PyMC** [14] packages.

4.5   Experimental Plan for Cavity Scan

Finally, in order to apply knowledge learned from the simulations above, we must have a method for measuring the transmission spectrum of an actual GW interferometer. In this section, we describe a technique for experimentally measuring the mode spacings of an optical cavity as outlined in [15].

In this method, one main laser beam and one auxiliary beam are injected into the optical setup from the dark port. The two beams are set to different frequencies, which are stabilized by a servo in the phased-locked loop (PLL). As in our simulation above, a photodector connected to a RF analyzer is used to read the transmission of the cavity. When the auxiliary beam is at a resonant frequency of the cavity, frequency beating appears in the cavity transmission. Thus, the mode spacings of the cavity can be read directly from the LO frequency of the PLL when the cavity transmission is at its maximum.
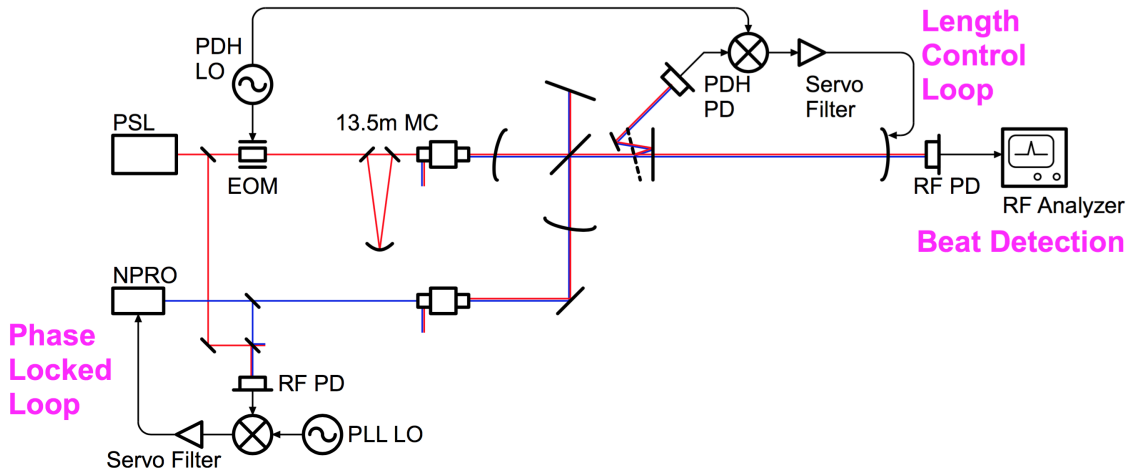

Figure 13: Optical setup for measuring cavity mode spacings. Source: [15]

As the frequency of the PLL LO is swept over a range of around 20 MHz, several equally-spaced peaks will appear in the measurement of transmitted light amplitude. Each peak can be fit using the formula

$$V(f) = \frac{A}{\sqrt{1 - \frac{(f-f_o)^2}{f_c^2}}}, \tag{22}$$

where f is the input frequency and A, f_0, and f_c are parameters. Once fit, the frequencies of each peak will be related linearly; the spacing between them is the free spectral range, ν_{FSR}. Once this spacing is found, we can use Equation (5) to calculate the approximate length (L) of the cavity.

To measure the transverse mode spacings of the cavity, we can insert a razor blade into the setup such that it blocks half of the beam either horizontally or vertically. In addition, the

auxiliary beam described above is misaligned. Both of these processes allow the first order Hermite-Gaussian modes ($\text{TEM}_{01/10}$) to appear in the cavity transmission measurement. Once again, we can fit these peaks and determine the spacing between adjacent peaks. Using Equation (9) and the measured ν_{FSR} from the TEM_{00} mode, we can then calculate the radius of curvature of the cavity mirror. In addition, if the $\text{TEM}_{01/10}$ modes have different resonance frequencies, indicating different radii of curvature in the horizontal and vertical directions, we can diagnose the mirror as astigmatic.

5   Acknowledgements

Appendix A. Hermite Polynomials

The Hermite polynomials are an infinite sequence of orthogonal polynomials. The Hermite polynomial of order n can be found by the generating function [6]:

$$e^{2xt-t^2} = \sum_{n=0}^{\infty} \frac{H_n(x)t^n}{n!}.$$ (23)

The first several Hermite polynomials are listed below:

order (n)	$H_n(x)$
0	1
1	$2x$
2	$4x^2 - 2$
3	$8x^3 - 12x$
4	$16x^4 - 48x^2 + 12$
5	$32x^5 - 160x^3 + 120x$

Appendix B. Zernike Polynomials

The Zernike polynomials are an infinite sequence of polynomials that are orthogonal on the unit disk, characterized by two indices (n, m). The first several Zernike polynomials Z_n^m are listed below:

radial order (n)	azimuthal order (m)	$Z(\rho, \theta)$
0	0	1
1	1	$2\rho \cos\theta$
1	-1	$2\rho \sin\theta$
2	0	$\sqrt{3}(2\rho^2 - 1)$
2	-2	$\sqrt{6}\rho^2 \sin 2\theta$
2	2	$\sqrt{6}\rho^2 \cos 2\theta$
3	-1	$\sqrt{8}(3\rho^3 - 2\rho) \sin\theta$
3	1	$\sqrt{8}(3\rho^3 - 2\rho) \cos\theta$
3	-3	$\sqrt{8}\rho^3 \sin 3\theta$
3	3	$4\sqrt{8}\rho^3 \cos 3\theta$

Appendix C. Bayes' theorem of inverse problems

The following is quoted from [10], p. 51:

Bayes' theorem of inverse problems: *Assume that the random variable $X \in \mathbb{R}^n$ has a known prior probability density $\pi_{pr}(x)$ and the data consist of the observed value y_{observed}*

of an observable random variable $Y \in \mathbb{R}^k$ *such that* $\pi(y_{\text{observed}}) > 0$. *Then the posterior probability distribution of* X, *given the data* y_{observed}, *is*:

$$\pi_{\text{post}}(x) = \pi(x \mid y_{\text{observed}}) = \frac{\pi_{\text{pr}}(x)\pi(y_{\text{observed}} \mid x)}{\pi(y_{\text{observed}})}. \tag{24}$$

References

[1] G. Vajente, *Introduction to GW detectors.* https://dcc.ligo.org/LIGO-G1701153

[2] *LIGO Caltech.* https://www.ligo.caltech.edu/page/ligos-ifo

[3] G. Billingsley, H. Yamamoto, and L. Zhang, *Characterization of Advanced LIGO Core Optics.* https://dcc.ligo.org/LIGO-P1700029

[4] B. E. A. Saleh and M. C. Teich, *Fundamentals of Photonics.* (John Wiley & Sons, 1991)

[5] D. Morin, *Waves.* Chapter 6: Dispersion. http://www.people.fas.harvard.edu/~djmorin/waves/dispersion.pdf

[6] A. E. Siegman, *Lasers.* (University Science Books, 1986)

[7] A. Stochino, K. Arai, and R. X. Adhikari, *A Technique for In-situ Measurement of Free Spectral Range and Transverse Mode Spacing of Optical Cavities.* (Applied Optics, 2012)

[8] *Finesse.* http://www.gwoptics.org/finesse/

[9] *LIGO 40m Wiki: Core Optics.* https://wiki-40m.ligo.caltech.edu/Core_Optics

[10] J. Kaipio and E. Somersalo, *Statistical and Computational Inverse Problems.* (Springer Science+Business Media, 2005)

[11] J.-M. Marin and C. P. Robert, *Bayesian Core: A Practical Approach to Computational Bayesian Statistics.* (Springer Science+Business Media, 2007)

[12] S. S. Qian, C. A. Stow, and M. E. Borsuk, *On Monte Carlo methods for Bayesian inference.* Ecological Modelling 159:269-277, 2003.

[13] *emcee Documentation.* http://dfm.io/emcee/current/

[14] *PyMC Documentation.* https://pymc-devs.github.io/pymc/

[15] K. Arai, A. Stochino, R. Adhikari, and the LIGO 40m Lab, *Precise Measurements on Longitudinal and Transverse Mode Spacings of an Optical Cavity using an Auxiliary Laser.* https://dcc.ligo.org/LIGO-G080467